NeuroImage 280 (2023) 120333

Contents lists available at ScienceDirect

NeuroImage

journal homepage: www.elsevier.com/locate/ynimg

PSIICOS projection optimality for EEG and MEG based functional coupling detection

Dmitrii Altukhov [b,1], Daria Kleeva [a,1], Alexei Ossadtchi [a,b,c,*,1]

[a] Center for Bioelectric Interfaces, Higher School of Economics, Moscow, Russia
[b] AIRI, Artificial Intelligence Research Institute, Moscow, Russia
[c] LLC "Life Improvement by Future Technologies Center", Moscow, Russia

ARTICLE INFO

Keywords:
MEG
EEG
Connectivity
Dynamic networks
Cross-spectrum
Spatial leakage
Optimization

ABSTRACT

Functional connectivity is crucial for cognitive processes in the healthy brain and serves as a marker for a range of neuropathological conditions. Non-invasive exploration of functional coupling using temporally resolved techniques such as MEG allows for a unique opportunity of exploring this fundamental brain mechanism.

The indirect nature of MEG measurements complicates the estimation of functional coupling due to the volume conduction and spatial leakage effects. In the previous work (Ossadtchi et al., 2018), we introduced PSIICOS, a method that for the first time allowed us to suppress the volume conduction effect and yet retain information about functional networks whose nodes are coupled with close to zero or zero mutual phase lag.

In this paper, we demonstrate analytically that the PSIICOS projection is optimal in achieving a controllable trade-off between suppressing mutual spatial leakage and retaining information about zero- or close to zero-phase coupled networks. We also derive an alternative solution using the regularization-based inverse of the mutual spatial leakage matrix and show its equivalence to the original PSIICOS.

We then discuss how PSIICOS solution to the functional connectivity estimation problem can be incorporated into the conventional source estimation framework. Instead of sources, the unknowns are the elementary dyadic networks and their activation time series are formalized by the corresponding source-space cross-spectral coefficients. This view on connectivity estimation as a regression problem opens up new opportunities for formulating a set of principled estimators based on the rich intuition accumulated in the neuroimaging community.

In support of academic freedom this paper has been accepted for publication during a war in which Russia invaded Ukraine. The Senior Editorship of NeuroImage condemns this act of violence.

1. Introduction

Functional connectivity, which refers to the interaction and communication between different brain regions, plays a crucial role in understanding various cognitive processes taking place in the brain (Greicius, 2008; Hutchison et al., 2013). Non-invasive techniques like magnetoencephalography (MEG) and electroencephalography (EEG) have greatly aided research in this field. These techniques provide high temporal resolution, which allows researchers to investigate various types of functional coupling between neuronal population activity time series. This includes identifying types of functional coupling that are marked by phase synchrony and distributed across different frequency bands (Siegel et al., 2012). The cross-spectrum is frequently utilized to calculate functional connectivity between two narrow band neuronal time series (Gail et al., 2004; Zeitler et al., 2006; Bastos and Schoffelen, 2016). As shown in Aydore et al. (2013) the absolute value of the normalized cross-spectrum measures the degree of phase coupling between a pair of circularly Gaussian random processes. Therefore, according to the *communication through coherence* principle (Fries, 2015; Varela et al., 2001), the coherence is often used to gauge the amount of communication between a pair of neuronal populations (Bowyer, 2016).

Investigating brain function using non-invasive, time-resolved imaging methods such as EEG and MEG offers access to a great level of details regarding the dynamics of neuronal activity combined with the versatility of the iterative experimental design. EEG and MEG represent indirect measurements of brain activity and yield multivariate time series where each channel represents a mixture of activity of individual neuronal sources. Due to fundamental limitation of the electromagnetic

* Corresponding author at: Center for Bioelectric Interfaces, Higher School of Economics, Moscow, Russia.
E-mail address: ossadtchi@gmail.com (A. Ossadtchi).
[1] All authors contributed equally to the work.

https://doi.org/10.1016/j.neuroimage.2023.120333
Received 25 March 2023; Received in revised form 12 July 2023; Accepted 14 August 2023
Available online 22 August 2023

inverse problem the attempted unmixing is not perfect and the residual common components in the obtained source activity estimates result in spurious interactions between reconstructed sources, known as spatial leakage (SL). The SL hinders estimation of the cross-spectral coefficients between neuronal sources based on such non-invasively collected EEG and MEG. To partially resolve this problem, functional coupling estimation is typically preceded by a source time series estimation step using one of the numerous inverse solvers developed by the community over the last several decades (Samuelsson et al., 2021; Westner et al., 2022). The role of this step is to "unmix" the sensor data and gain access to the activation time series of the individual neuronal sources, approximated by equivalent current dipoles (ECDs). The inverse problem of EEG and MEG is fundamentally ill-posed, which means that no inverse method can achieve perfect unmixing. The estimated sources and the spatial resolution of these estimates are influenced by factors such as the signal-to-noise ratio, location and orientation of the sources. Choosing an inverse operator involves a trade-off between localization error and spatial dispersion (Samuelsson et al., 2021). Even if an estimator is designed to produce a distribution with its peak aligned to the true active source, it can still be affected by false leakage from other sources. This is particularly observed in deep brain regions, which may receive signals from superficial sources (Hauk et al., 2022).

In the functional connectivity (FC) analysis context, source estimation fidelity does not automatically translate into the accuracy of the FC estimates. As pointed in Hincapie et al. (2017) the best source activity and FC estimation results are obtained by the MNE inverse operators computed with two different regularization parameters. This happens because the accuracy of the FC estimate between a pair of sources depends not so much on the CTF of an individual source but rather on the mutual alignment of the CTFs of these two sources. In other words, the FC estimation based on the indirect non-invasive measurements of brain activity is biased by the contribution of common sources to the estimates of activity of a pair of sources (i, j) assessed for functional interaction. Formally, the amount of such common contribution can be computed as a scalar product of the ith and jth rows of resolution matrix $\mathbf{R}$ described in Samuelsson et al. (2021) and needs to be minimized in order to obtain accurate FC estimates. Such a minimization of the overlap between the two CTFs corresponding to the ith and jth source requires simultaneous design of the two spatial filters extracting the activity of the ith and jth sources for the FC estimation needs.

In Ossadtchi et al. (2018) we have introduced a method called PSIICOS (Phase shift invariant imaging of coherent sources). PSIICOS treats $M \times M$ complex-valued sensor-space cross-spectrum as an $M^2 \times 1$ vector and then exploits linear-algebra theoretic approach to suppress the SL and estimate both real and imaginary elements of the source-space cross-spectrum. As demonstrated with realistic simulations and in application to real MEG data, the PSIICOS methodology augments more traditional approaches (Nolte et al., 2004; Stam et al., 2007; Nolte et al., 2008; Pascual-Marqui et al., 2011; Ewald et al., 2012) by adding sensitivity to functional networks with zero or close-to-zero phase coupling.

In this paper we perform an in-depth analysis of PSIICOS and show that it can be derived as an optimal solution simultaneously tuning two spatial filters to minimize the amount of overlap between the pair of CTFs corresponding to two cortical sources tested for functional coupling. We first introduce a new criterion, called mutual spatial leakage (MSL), that is conceptually similar to the scalar product of the ith and jth rows of $\mathbf{R}$ but computed using the rows of matrix $\mathbf{B}^{\odot 2} = \{r_{ij}^2\}$ whose elements are simply the squares of the corresponding entries of the resolution matrix $\mathbf{R}$ defined in Samuelsson et al. (2021). The use of squares gives us additional analytical freedom and allows for deriving PSIICOS as the optimal approach that minimizes the amount of the MSL.

Next using two regularization techniques, Moore–Penrose and Tikhonov, we arrive at two solutions that minimize the MSL and align with the original PSIICOS solution. We also illustrate the criterion to gauge the trade-off between the MSL suppression and retention of the spatial components (in the M^2 dimensional space) modulated by the real part of the source space cross-spectral coefficients carrying information about close to zero and zero-phase coupled elementary dyadic networks. The trade-off can be tuned using projection rank and the regularization parameter respectively.

Interestingly, the treatment of sensor-space covariance matrix as an $M^2 \times 1$ vector allows us to view the source-space coupling detection as a linear regression problem. In the final section of the paper we discuss the implications of such a treatment and propose directions for development of the new generation of FC analysis methods.

Finally, in the Discussion we summarize our development, draw some additional intuition and link PSIICOS to several other approaches aimed at reducing the cross-talk in the context of source-space coupling estimation.

2. Spatial leakage and its suppression by means of orthogonal projection in the product space of sensor signals

2.1. Generative models of the sensor signals

The EEG/MEG experimental setup involves recording K epochs of electrophysiological activity using an M-channel encephalographic device. The subject's brain anatomy, either from a generic head model or an individual MRI scan, defines the source space, a mesh approximating the cortical surface, so that each of total N vertices harbors a neuronal source approximated by the equivalent current dipole (ECD). The $M \times N$ forward operator $\mathbf{G} = \{\mathbf{g}_i\},\ i = 1, \ldots, N$ at each kth trial maps the activity $s_i^k(t),\ i = 1, \ldots, N$ of these ECDs to the $M \times 1$ vector of sensor-space measurements $\mathbf{x}^k(t)$. The data are then corrupted by $M \times 1$ additive noise vector $\mathbf{n}^k(t)$. Thus, assuming for each of K trials identical configuration of N active sources, the following generative equation for the data observed at time instance t within the kth trial:

$$\mathbf{x}^k(t) = \sum_{i=1}^{N} \mathbf{g}_i s_i^k(t) + \mathbf{n}^k(t), \tag{1}$$

where $M \times 1$ vector $\mathbf{g}_i$ denotes the ith column of forward operator $\mathbf{G}$, representing the topography of the ith source, and $\mathbf{n}^k(t) \sim \mathcal{N}(0, \mathbf{R}_n)$ models zero mean additive noise with spatial covariance $\mathbf{R}_n$ during the kth epoch. The noise is assumed uncorrelated between epochs, i.e. $E\{\mathbf{n}^k(t)\mathbf{n}^l(t)\} = 0,\ k \neq l$.

It is implicitly assumed that only a small fraction of N sources is active and the summation in (1) can be replaced by a smaller summation over a subset Ω of active sources. However, since the subset of active sources is unknown, we will stick to the more general formulation as presented above so that inactive sources are assumed to have $s_i^k(t) = 0$ over the duration of the kth trial.

Networks analysis is traditionally performed via two steps. At first one uses an inverse solver to obtain estimates of the source activation profiles $s_i(t)$. Once this is done, within the second step the functional coupling metrics are computed to analyze the functional networks of interest.

To analyze within frequency linear synchronization we typically for each pair of source time series estimates $s_i(t)$ and $s_j(t)$ compute the coherence function coh_{ij} defined as the normalized squared cross-spectral coefficient and is a function of frequency, i.e.

$$coh_{ij}^{ss}(f,t) = \frac{\left|E\{\overline{S_i(f,t)}S_j(f,t)\}\right|^2}{E\{\overline{S_i(f,t)}S_i(f,t)\}E\{\overline{S_j(f,t)}S_j(f,t)\}} = \frac{|c_{ij}^{ss}(f,t)|^2}{c_{ii}^{ss}(f,t)c_{jj}^{ss}(f,t)} \tag{2}$$

where $S_i(f,t)$ is the time–frequency representation of the ith source time series and $c_{ij}^{ss}(f,t)$ are the elements of the source space (note ss superscript) cross-spectral matrix $\mathbf{C}^{ss}(f,t) = \{c_{ij}^{ss}(f,t)\} = E\{\mathbf{S}(f,t)\mathbf{S}^H(f,t)\}$ where $\mathbf{S}(f,t) = [S_1(f,t), \ldots, S_N(f,t)]^T$ is a vector of time–frequency transformed source activation time series $s_i(t)$ for $i = 1, \ldots, N$, t indexes the time within a trial and f is the frequency of interest. Averaging

across K trials yields an estimate of the true coherence between source time series. In practice the actual source time series in (2) are replaced with their estimates and the expectation operation is replaced by averaging across trials for stimulus-based paradigms or across time within a sliding window for the resting-state data analysis. Both techniques allow us to retain the temporal dimension of coherence and subsequently analyze it as a time-varying function. The coherence is computed using the elements of the cross-spectral matrix capturing the information about linear coupling of sources with normally distributed time series. For a comprehensive examination of the implications of non-Gaussian components in electrophysiological signals on functional coupling detection, please refer to Hindriks and Tewarie (2023).

2.2. Generative model for the cross-spectral matrix

PSIICOS relies on the generative equation linking the source and sensor-space cross-spectral matrices. Applying a time–frequency transform (typically wavelet transform) to both sides of (1) and exploiting the transform's linearity we will obtain the following expression for the time–frequency transformed sensor signals

$$\mathbf{X}^k(f,t) = \sum_{i=1}^{N} \mathbf{g}_i S_i^k(f,t) + \mathbf{N}^k(f,t), \tag{3}$$

Then, by applying the definition of the cross-spectral matrix to the time–frequency transformed sensor data (3) we obtain the following generative model of the sensor space cross-spectrum $\mathbf{C}^{XX}(f,t)$ linking it to the source space cross-spectral matrix $\mathbf{C}^{ss}(f,t)$:

$$\mathbf{C}^{XX}(f,t) = E\{\mathbf{X}(f,t)\mathbf{X}^H(f,t)\} = \mathbf{G}\mathbf{C}^{ss}(f,t)\mathbf{G}^T + \mathbf{C}^{NN}(f,t). \tag{4}$$

Here $\mathbf{C}^{NN}(f,t)$ is the cross-spectral matrix of the additive noise and $\mathbf{C}^{ss}(f,t) = E\{\mathbf{S}(f,t)\mathbf{S}^H(f,t)\}$. The approximation of the expectation operation $E\{\}$ is computed by averaging the products of time–frequency coefficient matrices over K trials.

2.3. Manifestation of the SL effect in the cross-spectrum

Similarly to the way it was done in Ossadtchi et al. (2018) we expand matrix products in (4) into the summations of the modulated outer products of topographies and split the real and imaginary parts to obtain:

$$\begin{aligned}\mathbf{C}^{XX}(f,t) = &\sum_{i=1}^{N} \mathbf{g}_i\mathbf{g}_i^T c_{ii}^{ss}(f,t) + \sum_{i=1}^{N}\sum_{j=i+1}^{N} \left(\mathbf{g}_i\mathbf{g}_j^T + \mathbf{g}_j\mathbf{g}_i^T\right) \Re(c_{ij}^{ss}(f,t)) + \\ &+ \mathrm{i}\left[\sum_{i=1}^{N}\sum_{j=i+1}^{N} \left(\mathbf{g}_i\mathbf{g}_j^T - \mathbf{g}_j\mathbf{g}_i^T\right) \Im(c_{ij}^{ss}(f,t))\right] \\ &+ \mathbf{C}^{NN}(f,t)\end{aligned} \tag{5}$$

Let us now consider the diagonal of the source space cross-spectrum matrix $\mathbf{C}^{\mathbf{ss}}(f,t) = \{c_{ij}^{ss}(t,f)\}$ in more detail. The elements $c_{ii}^{ss}(t,f)$, $i = 1,\ldots,M$ of the main diagonal of this matrix are real numbers and they represent the power of source activation time series around frequency f at time t. The structure of the generative model reflects the fact that after being mapped from the source space to the sensor space using the operator $\mathbf{G}$, these power terms will manifest themselves both in the diagonal and off-diagonal elements of the sensor-space cross-spectral matrix $\mathbf{C}^{\mathbf{xx}}(f,t)$. The kth row of matrix $\mathbf{G}$ corresponds to the lead field of the kth sensor and describes how the activity of neuronal sources gets mixed in the sensor measurements.

The symmetric matrices $(\mathbf{g}_i\mathbf{g}_i^T)$ map the diagonal elements of the source-space cross-spectrum matrix (source powers) onto the sensor-space cross-spectrum, another set of symmetric matrices $(\mathbf{g}_i\mathbf{g}_j^T + \mathbf{g}_j\mathbf{g}_i^T)$ carries information about the *real* part of the off-diagonal source space cross-spectrum elements, while the anti-symmetric matrices $(\mathbf{g}_i\mathbf{g}_j^T - \mathbf{g}_j\mathbf{g}_i^T)$ map the *imaginary* part of the off-diagonal elements, $\Im(c_{ij}^{ss})$.

The orthogonality of symmetric and anti-symmetric matrices and the subspaces of real and imaginary parts of cross-spectrum, as well as sensitivity of the imaginary part of cross-spectrum to time-lagged interactions, leads to the independence of the imaginary part of the sensor-space cross-spectrum from the instantaneously occurring spatial leakage. This observation led to the development of several SL-invariant functional coupling metrics (Nolte et al., 2004; Stam et al., 2007; Nolte et al., 2008; Pascual-Marqui et al., 2011; Ewald et al., 2012). These elegant solutions come at a price of neglecting the functional networks whose time series exhibit zero or close-to-zero mutual phase lag.

PSIICOS suggests a less radical approach and instead of using solely the imaginary part of the cross-spectrum, PSIICOS suggests vectorizing $\mathbf{C}^{XX}(f,t)$ and representing it as a linear superposition of 2-topographies $\mathbf{q}_{ij} = vec(\mathbf{g}_i\mathbf{g}_j^T) = \mathbf{g}_j \otimes \mathbf{g}_i^T$:

$$\begin{aligned}vec(\mathbf{C}^{XX})(f,t) = &\sum_{i=1}^{N} \mathbf{q}_{ii} c_{ii}^{ss}(f,t) + \sum_{i=1}^{N}\sum_{j=i+1}^{N} \left(\mathbf{q}_{ij} + \mathbf{q}_{ji}\right) \Re(c_{ij}^{ss}(f,t)) + \\ &+ \mathrm{i}\left[\sum_{i=1}^{N}\sum_{j=i+1}^{N} \left(\mathbf{q}_{ij} - \mathbf{q}_{ji}\right) \Im(c_{ij}^{ss}(f,t))\right] \\ &+ vec(\mathbf{C}^{NN})(f,t)\end{aligned} \tag{6}$$

It is then easy to notice that the $M^2 \times 1$ vectorized complex-valued sensor-space cross-spectrum $vec(\mathbf{C}^{XX})(f,t)$ is a linear superposition of three components: (1) real-valued spatial leakage (SL), (2) real valued contribution of the true source space coupling and (3) imaginary contribution of the true source space coupling. Based on this observation, PSIICOS suggests the SVD-based recipe to identify a finite dimensional subspace of the M^2-dimensional space that dominantly captures the SL component power and then uses it to derive an $M^2 \times M^2$ projector matrix to be applied to the vectorized cross-spectrum $vec(\mathbf{C}^{XX})(f,t)$ in order to minimize the contribution of the SL (component 1) while retaining the information about zero or close-to-zero phase interactions stored in the real and imaginary parts of the source-space cross-spectral coefficients, components 2 and 3 correspondingly.

2.4. PSIICOS as an optimal filtering approach

It is important to note that the SL effect is not limited to the cross-talk only between the two sources for which the connectivity is being measured. Any source that leaks into the estimate of activity for both of these sources simultaneously will potentially result in erroneous estimates. As a special case, the third source leaking into only one of the target sources may bias the estimation of coherence as well, because this leakage changes the power of the target source used then to compute the coherence coefficient. Therefore, in order to accurately evaluate connectivity between a pair of sources, it is in general necessary to design a set of spatial filters that maximally suppress cross-talk from sources that are simultaneously leaking into the estimates of activity for both target sources.

To quantify the amount of such leakage we can use the concept of resolution kernel (RK) $R(\mathbf{r},\mathbf{r}')$ introduced in the theory of inverse problems and used in Sekihara and Nagarajan (2008). Let us consider an inverse operator that recovers the activity at a point $\mathbf{r}$ in the cortex based on measurements from sensors, and fix another cortical point $\mathbf{r}'$. The function $R(\mathbf{r},\mathbf{r}')$ indicates the amount of signal that leaks from point $\mathbf{r}'$ into the estimate of activity of a source located at $\mathbf{r}$. For linear methods of solving the inverse problem, the function R can be expressed as a scalar product as follows:

$$R(i,k) = \mathbf{l}_i^T \mathbf{g}_k, \tag{7}$$

where $\mathbf{l}_i$ is the filter used to estimate the activity of the ith cortical source and $\mathbf{g}_k$ is the topography of the kth source.

We can define a vector-valued function $\mathbf{B}(i)$, where $i = 1,\ldots,N$, that quantifies the amount of signal flow from each cortical point to the fixed point i:

$$\mathbf{B}(i) = [R(i,1), R(i,2), \ldots, R(i,N)]^T \tag{8}$$

The function has been referred to as the Beam Response (BR) (Sekihara and Nagarajan, 2008) and when absolute values are taken it is equivalent to the row of resolution matrix described in Samuelsson et al. (2021). Conceptually, the BR is similar to the notion of a lead-field, which represents a row of the forward matrix that shows the sensitivity of a specific sensor to the activity of cortical sources. The major difference with the lead field is that the BR $\mathbf{B}(i)$ concerns not a specific sensor but rather a specific cortical location with index i. Vector $\mathbf{B}(i)$ reflects the amount of signal leaking from each cortical source into the estimate of activity of the ith *vertex*. In the ideal case, the ith element of $\mathbf{B}(i)$ is one, and the rest of its elements are zeros, i.e. $\mathbf{B}(i)_n = \delta(i-n)$, for $n = 1, \dots, N$.

Let us now consider two points i and j on the cortex. The degree of overlap between vectors $\mathbf{B}(i)$ and $\mathbf{B}(j)$ plays a crucial role in determining the magnitude of the shared component of the SL signal. In an ideal scenario, if the components of both vectors, $\mathbf{B}(i)$ and $\mathbf{B}(j)$, are non-negative and orthogonal to each other, the common mode signal flowing simultaneously through points i and j will be null, resulting in the elimination of the SL and its contribution to the connectivity estimate. This highlights the importance of designing a pair of filters that minimize the overlap between $\mathbf{B}(i)$ and $\mathbf{B}(j)$ for every pair of points (i, j).

In order to construct such filters, it is essential to establish a methodology for measuring the overlap between the vectors $\mathbf{B}(i)$ and $\mathbf{B}(j)$. The scalar product of these vectors may initially seem like an adequate measure of the overlap: if this measure is equal to zero, the common leakage is absent. However, this measure is flawed due to the potential sign change of the components of these vectors. Even though the scalar product between vectors $\mathbf{B}(i)$ and $\mathbf{B}(j)$ is zero, indicating that they are orthogonal, the individual components of these vectors may still be substantial and interfere with each other if they possess opposite signs. For instance, if the functions $\mathbf{B}$ are equal to $(1, -1)$ and $(1, 1)$ correspondingly for the points i and j, the BRs are orthogonal to each other, but the SL between the sources is significant.

To resolve this issue, a more accurate measure of overlap is required. The magnitude of the scalar product of the vectors $\mathbf{B}(i)$ and $\mathbf{B}(j)$ whose components are first squared, serves as a more appropriate measure of overlap. We will refer to the result of this scalar product, the function $\mu(i, j)$, as *mutual spatial leakage (mutual SL)* of the points i and j and formally define it as:

$$\mu(i,j) \stackrel{\text{def}}{=} (\mathbf{B}(i)^{\odot 2})^T \mathbf{B}(j)^{\odot 2} \tag{9}$$

where $(\cdot)^{\odot 2}$ notation is inspired by the Hadamard product and denotes squaring the corresponding vector element-wise. This measure is similar to that used in Nolte et al. (2009) for describing the constraints on the theoretical distribution of sources.

Taking into account the definition of resolution kernel (7), the mutual SL can be expanded as:

$$\mu(i,j) = \sum_k \left(\mathbf{l}_i^T \mathbf{g}_k\right)^2 \left(\mathbf{l}_j^T \mathbf{g}_k\right)^2 = \sum_k \left(\mathbf{l}_i^T \mathbf{g}_k \mathbf{g}_k^T \mathbf{l}_j\right)^2 = (\mathbf{l}_j \otimes \mathbf{l}_i)^T \mathbf{\Gamma}\mathbf{\Gamma}^T (\mathbf{l}_j \otimes \mathbf{l}_i),$$
$$\mathbf{\Gamma} = (\mathbf{g}_1 \otimes \mathbf{g}_1, \dots, \mathbf{g}_N \otimes \mathbf{g}_N), \tag{10}$$

note that $\mathbf{g}_j \otimes \mathbf{g}_i$ is the Kronecker product based notation equivalent to $vec(\mathbf{g}_i \mathbf{g}_j^T)$ used in the original PSIICOS paper (Ossadtchi et al., 2018). Importantly, the columns of Γ are vectorized symmetric matrices since $\mathbf{g}_k \otimes \mathbf{g}_k = vec(\mathbf{g}_k \mathbf{g}_k^T)$

With the aim of minimizing mutual SL while preserving the signal of interest, we seek to find a pair of filters $\mathbf{l}_i$, $\mathbf{l}_j$ for points i and j. To achieve this, it is necessary to impose additional constraints on the length and orientation of these spatial filters. One possible constraint is the requirement that the signal amplification coefficient for signals originating from points with topographies $\mathbf{g}_i$ and $\mathbf{g}_j$ is equal to 1. Taking into account this constraint, the optimization problem for finding the pair of filters $\mathbf{l}_i, \mathbf{l}_j$ can be written as follows:

$$\frac{1}{2}\mu(i,j) = \frac{1}{2}(\mathbf{l}_j \otimes \mathbf{l}_i)^T \mathbf{\Gamma}\mathbf{\Gamma}^T (\mathbf{l}_j \otimes \mathbf{l}_i) \to \min \tag{11}$$
$$s.t. : \mathbf{l}_i^T \mathbf{g}_i = 1, \mathbf{l}_j^T \mathbf{g}_j = 1$$

Under this constraint, the optimization problem cannot be explicitly solved by the method of Lagrange multipliers due to the presence of the Kronecker product in the objective function. Thus, it must be solved numerically, for example, by the gradient descent method. However, this problem can be significantly simplified generalizing the concept of filters to the M^2-dimensional space of the vectorized MEG or EEG data covariance matrices.

It should be noted that the constraints of (11) imply that

$$(\mathbf{l}_j \otimes \mathbf{l}_i)^T (\mathbf{g}_j \otimes \mathbf{g}_i) = 1 \tag{12}$$

Note that the constraint, written in such a form as the objective function in Eq. (11), depends on the filters $\mathbf{l}_i, \mathbf{l}_j$ only through their Kronecker product, which we denote as $\mathbf{v}_{ij}$. Importantly, such a general form of $\mathbf{v}_{ij}$ not only allows us to solve the optimization problem analytically but also yields a better solution than it is possible in case $\mathbf{v}_{ij}$ is restricted to be a Kronecker product of two M-dimensional vectors. See also Section 3 for a detailed analysis of the effect of restricting the structure of $\mathbf{v}_{ij}$.

For the sake of compactness, we also denote $\mathbf{g}_j \otimes \mathbf{g}_i$ as $\mathbf{q}_{ij}$ and refer to such M^2-dimensional "topography" of a dyadic network as 2-topography.

$$\frac{1}{2}\mathbf{v}_{ij}^T \mathbf{\Gamma}\mathbf{\Gamma}^T \mathbf{v}_{ij} \to \min \tag{13}$$
$$s.t. : \mathbf{v}_{ij}^T \mathbf{q}_{ij} = 1$$

Such a problem regarding the variable $\mathbf{v}_{ij}$ can be easily solved using the Lagrange multiplier method. Its Lagrangian can be written as follows:

$$L(\mathbf{v}_{ij}, \lambda) = \frac{1}{2}\mathbf{v}_{ij}^T \mathbf{\Gamma}\mathbf{\Gamma}^T \mathbf{v}_{ij} + \lambda(\mathbf{v}_{ij}^T \mathbf{q}_{ij} - 1) \tag{14}$$

Differentiating the Lagrangian with respect to $\mathbf{v}_{ij}$, we obtain:

$$\frac{\partial L(\mathbf{v}_{ij}, \lambda)}{\partial \mathbf{v}_{ij}} = \mathbf{\Gamma}\mathbf{\Gamma}^T \mathbf{v}_{ij} + \lambda \mathbf{q}_{ij} = 0 \tag{15}$$

If $\lambda \neq 0$, Eq. (15) has no solutions: the columns of the matrix $\mathbf{\Gamma}$ are vectorizations of symmetric matrices, the product $\mathbf{\Gamma}\mathbf{\Gamma}^T$ is a circulant symmetric matrix and thus the product $\mathbf{\Gamma}\mathbf{\Gamma}^T \mathbf{v}_{ij}$ is a symmetric vector, which is also a vectorization of a symmetric matrix; however, $\mathbf{q}_{ij}$ is not a vectorization of a symmetric matrix. The difference is in our case for $\lambda \neq 0$ we have an incongruent system of equations due to the described above special structure of matrix $\mathbf{\Gamma}$ and vector $\mathbf{q}_{ij}$. This means that we need to set $\lambda = 0$ and obtain the following equation for $\mathbf{v}_{ij}$:

$$\mathbf{\Gamma}\mathbf{\Gamma}^T \mathbf{v}_{ij} = 0 \tag{16}$$

It follows that the vector $\mathbf{v}_{ij}$ must belong to the orthogonal complement of $col\ \mathbf{\Gamma}$, the column space of $\mathbf{\Gamma}$. This means that the vector $\mathbf{v}_{ij}$ can be obtained as the result of applying the projection $\mathbf{P} = \mathbf{I} - \mathbf{\Gamma}\mathbf{\Gamma}^\dagger$ to some vector $\tilde{\mathbf{v}}_{ij}$ from the general linear space of dimension M^2 ($\dagger$ denotes pseudoinverse).

Differentiating the Lagrangian in Eq. (14) with respect to λ results in:

$$\frac{\partial L(\mathbf{v}_{ij}, \lambda)}{\partial \lambda} = \mathbf{v}_{ij}^T \mathbf{q}_{ij} - 1 = 0 \tag{17}$$

Taking into account the general form of the vector $\mathbf{v}_{ij}$, as well as symmetry and idempotency of the projection operator $\mathbf{P}$, i.e. $\mathbf{P}^T\mathbf{P} = \mathbf{P}\mathbf{P} = \mathbf{P}$ we will obtain:

$$\tilde{\mathbf{v}}_{ij}^T \mathbf{P}^T \mathbf{q}_{ij} = \tilde{\mathbf{v}}_{ij}^T \mathbf{P}\mathbf{q}_{ij} = \tilde{\mathbf{v}}_{ij}^T \mathbf{P}^2 \mathbf{q}_{ij} = (\mathbf{P}\tilde{\mathbf{v}}_{ij})^T \mathbf{P}\mathbf{q}_{ij} = \mathbf{v}_{ij}^T \mathbf{P}\mathbf{q}_{ij} = 1 \tag{18}$$

The last equation defines a hyperplane in the affine subspace of vectors orthogonal to the columns of the matrix $\mathbf{\Gamma}$. As a result, the optimization problem has an infinite number of solutions. To choose

a unique solution, we can use the criterion of minimal norm as previously. Among the vectors of this hyperplane, the one with the minimum norm satisfying (18) has to be the vector collinear to $\mathbf{Pq}_{ij}$:

$$\mathbf{v}_{ij} = \frac{\mathbf{Pq}_{ij}}{\|\mathbf{Pq}_{ij}\|^2} = \frac{\mathbf{Pq}_{ij}}{\mathbf{q}_{ij}^T\mathbf{Pq}_{ij}} \tag{19}$$

Therefore, the filter that minimizes mutual SL for cortical points i, j is obtained as a result of the projection $\mathbf{P}$ applied to the corresponding 2-topography. Namely this projection was previously described and evaluated in Ossadtchi et al. (2018) where the authors basically suggest first to project the vectorized cross-spectrum $vec\left(\mathbf{C}^{XX}(f,t)\right)$ using operator $\mathbf{P}$ and then perform a scan using $\mathbf{Pq}_{ij}$ vectors, see Figure 1 in Ossadtchi et al. (2018). Due to idempotency of $\mathbf{P}$ this is equivalent to using filter (19).

In Ossadtchi et al. (2018) the authors applied PSIICOS to estimating the real and imaginary part of the source-space cross-spectrum separately which leads to the normalization imbalance when using the real and imaginary parts simultaneously. To address this issue, we modify the constraint in (13) to read as $\mathbf{v}_{ij}^T(\mathbf{q}_{ij}+\mathbf{q}_{ji}) = 1$ and for $\lambda = 0$ obtain the optimal filter to recover the real-part of the sources space cross-spectral coefficient $\Re(c_{ij}^{ss})$:

$$\mathbf{v}_{ij}^{Re} = \frac{\mathbf{P}(\mathbf{q}_{ij}+\mathbf{q}_{ji})}{(\mathbf{q}_{ij}+\mathbf{q}_{ji})^T\mathbf{P}(\mathbf{q}_{ij}+\mathbf{q}_{ji})} \tag{20}$$

Note that since $\mathbf{q}_{ij}+\mathbf{q}_{ji}$ is symmetric, for $\lambda \neq 0$ we will also have a solution for (15) that is very similar to the one we will obtain with Tikhonov regularization in Section 2.5.

For the imaginary part the constraint is $\mathbf{v}_{ij}^T(\mathbf{q}_{ij}-\mathbf{q}_{ji}) = 1$ which leads to the following filter:

$$\mathbf{v}_{ij}^{Im} = \frac{\mathbf{P}(\mathbf{q}_{ij}-\mathbf{q}_{ji})}{(\mathbf{q}_{ij}-\mathbf{q}_{ji})^T\mathbf{P}(\mathbf{q}_{ij}-\mathbf{q}_{ji})} \tag{21}$$

Since $(\mathbf{q}_{ij}-\mathbf{q}_{ji})$ and the column space of $\mathbf{\Gamma}$ are orthogonal, (21) can be restated as

$$\mathbf{v}_{ij}^{Im} = \frac{\mathbf{q}_{ij}-\mathbf{q}_{ji}}{\|\mathbf{q}_{ij}-\mathbf{q}_{ji}\|^2} \tag{22}$$

Note that in the limiting case when the number of cortical nodes exceeds the value $M(M+1)/2$, equal to the total number of symmetric $M \times M$ matrices, the application of operator $\mathbf{P}$ completely nullifies the vectorized symmetric matrices. This is effectively equivalent to taking the imaginary part of the cross-spectrum, as the imaginary parts of the antisymmetric topographies are antisymmetric and remain unchanged under projection.

In practice we operate with MEG or EEG time series data projected into a lower dimensional principal subspace of the forward model matrix $\mathbf{G}$. Typically, for EEG and MEG the rank of this subspace falls in 60 to 150 range. In MEG, when dealing with MaxFilter processed planar magnetometer data, the resulting rank is typically chosen to be below 100. If we consider a 73×73 matrix that is symmetric, the total number of such matrices is given by $n = 73\times(73+1)/2 = 2701$. Therefore, even for a relatively sparse cortical mesh with greater than n vertices, application of the full rank $\mathbf{P}$ to the sensor-space cross-spectrum will eliminate any information about the real-valued component of the cross-spectrum, see Fig. 1.b.

To balance the trade-off between the SL suppression and retention of the information about the real components of the source-space cross-spectrum we limit the projection rank R. Rank-limited $\mathbf{P}^R$ is computed using the first R left singular vectors $\mathbf{u}_i$, $i = 1, \ldots, R$ of $\mathbf{\Gamma}$ corresponding to the first R largest singular values as

$$\mathbf{P}^R = \mathbf{I} - \mathbf{U}_{1:R}\mathbf{U}_{1:R}^T \tag{23}$$

where $\mathbf{U}_{1:R} = [\mathbf{u}_1, \mathbf{u}_2, \ldots \mathbf{u}_R]$

In Fig. 1 we show the average suppression the PSIICOS projection bestows upon the spatial leakage (SL), real (Re) and imaginary (Im) 2-topographies for different projection ranks R. To obtain these plots we performed 10,000 Monte-Carlo (MC) trials. At each we randomly chose vertex index pairs (i, j) and computed the ratio of the post- to pre- projection norms of the corresponding 2-topographies $\mathbf{g}_i \otimes \mathbf{g}_i + \mathbf{g}_j \otimes \mathbf{g}_j$, $\mathbf{g}_i \otimes \mathbf{g}_j + \mathbf{g}_j \otimes \mathbf{g}_i$ and $\mathbf{g}_i \otimes \mathbf{g}_j - \mathbf{g}_j \otimes \mathbf{g}_i$. As expected, the 2-topographies corresponding to the imaginary part of true source space coherence appeared to be not affected by the PSIICOS projection, see the horizontal green curve in all three panels of the figure. For the 2-topographies corresponding to the SL component (blue curves) the suppression rapidly grows (attenuation factor decreases) with the rank increase while Re components are only reasonably suppressed. The comparison of these two curves allows us to assess the increase in the salience Re component with respect to the spatial leakage terms. To compare we subtract the attenuation factor of the SL component from that of Re component and obtain Re-SL difference curve shown in red. First, the increase of the projection rank leads to the more rapid increase of the SL suppression as compared to that of the Re component and the suppression difference curve grows. The difference curves peak at $R^{NMG.grad} = 400$, $R^{NMG.mag} = 200$ for the Neuromag with two sensor types and CTF probes correspondingly. This peak corresponds to the point where further increase of the projection rank leads to a more rapid depletion of power from Re components reflecting true coupling as compared to the SL components. The corresponding projection rank can be chosen as optimal.

2.5. Regularized PSIICOS solution

As already noted, with a sufficiently large number of cortical points, $\mathbf{P}$ constructed without the projection rank restriction completely eliminates information about the real parts of the source space cross-spectral matrix off-diagonal elements. Limiting the projection rank allowed us to manipulate the trade-off between the SL suppression and Re components power retention. In the previous derivation we have chosen the unique solution using the standard minimum-norm argument, see (19).

Here we consider an alternative way of formulating and solving the PSIICOS optimization problem. The approach is based on the Tikhonov regularization and allows us to simultaneously balance between the minimum norm and minimal leakage requirements. The optimization problem in this case is written as

$$\begin{aligned} &\frac{1}{2}\mathbf{v}_{ij}^T\mathbf{\Gamma}\mathbf{\Gamma}^T\mathbf{v}_{ij} + C\frac{1}{2}\|\mathbf{v}_{ij}\|^2 \rightarrow \min \\ &s.t. : \mathbf{v}_{ij}^T\mathbf{q}_{ij} = 1 \end{aligned} \tag{24}$$

where $C\frac{1}{2}\|\mathbf{v}_{ij}\|^2$ allows for a soft control over the norm of the obtained PSIICOS filter vector.

The Lagrangian for this optimization problem is

$$L(\mathbf{v}_{ij}, \lambda) = \frac{1}{2}\mathbf{v}_{ij}^T\mathbf{\Gamma}\mathbf{\Gamma}^T\mathbf{v}_{ij} + C\frac{1}{2}\|\mathbf{v}_{ij}\|^2 + \lambda(\mathbf{v}_{ij}^T\mathbf{q}_{ij} - 1) \tag{25}$$

Taking the derivative with respect to $\mathbf{v}_{ij}$ we get:

$$\frac{\partial L(\mathbf{v}_{ij}, \lambda)}{\partial \mathbf{v}_{ij}} = \mathbf{\Gamma}\mathbf{\Gamma}^T\mathbf{v}_{ij} + C\mathbf{v}_{ij} + \lambda\mathbf{q}_{ij} = 0 \tag{26}$$

This time, thanks to the regularization (26) has solutions for non-zero λ

$$\mathbf{v}_{ij} = -\lambda(\mathbf{\Gamma}\mathbf{\Gamma}^T + C\mathbf{I})^{-1}\mathbf{q}_{ij} \tag{27}$$

Multiplying the left and the right parts by $\mathbf{q}_{ij}$ and taking into account the constraint $\mathbf{v}_{ij}^T\mathbf{q}_{ij} = 1$, we get the expression for λ:

$$\lambda = -\frac{1}{\mathbf{q}_{ij}^T(\mathbf{\Gamma}\mathbf{\Gamma}^T + C\mathbf{I})^{-1}\mathbf{q}_{ij}} \tag{28}$$

The corresponding filter $\mathbf{v}_{ij}$ is then given by

$$\mathbf{v}_{ij} = \frac{(\mathbf{\Gamma}\mathbf{\Gamma}^T + C\mathbf{I})^{-1}\mathbf{q}_{ij}}{\mathbf{q}_{ij}^T(\mathbf{\Gamma}\mathbf{\Gamma}^T + C\mathbf{I})^{-1}\mathbf{q}_{ij}} \tag{29}$$

As it turns out both (19) and (29) give nearly identical results for a broad range of the regularization parameter C, compare Figs. 1 and 2.

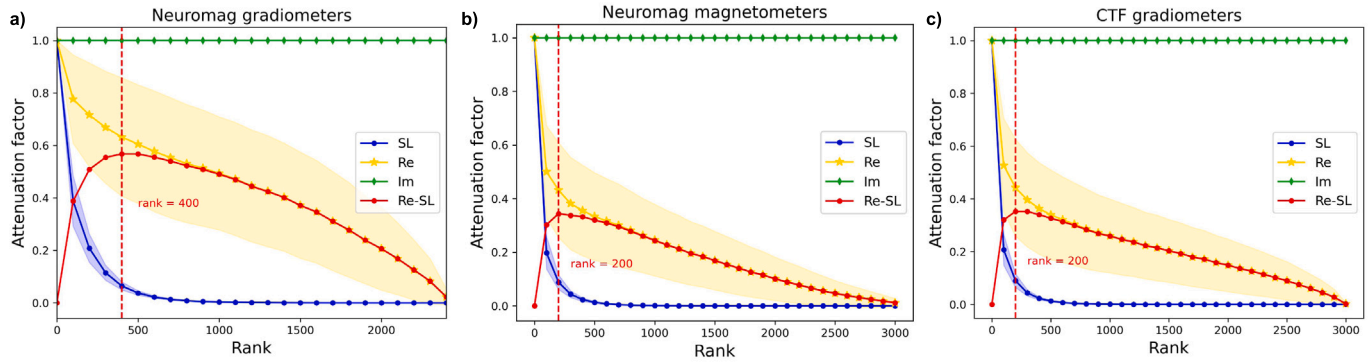

Fig. 1. SL and Re subspace power suppression and the suppression difference curve for the original (projected) PSIICOS as a function of projection rank (a) for Neuromag 204 planar gradiometers probe, (b) for Neuromag 102 magnetometers probe and (c) for 275 radial gradiometers CTF probe. (For interpretation of the references to colour in this figure legend, the reader is referred to the web version of this article.)

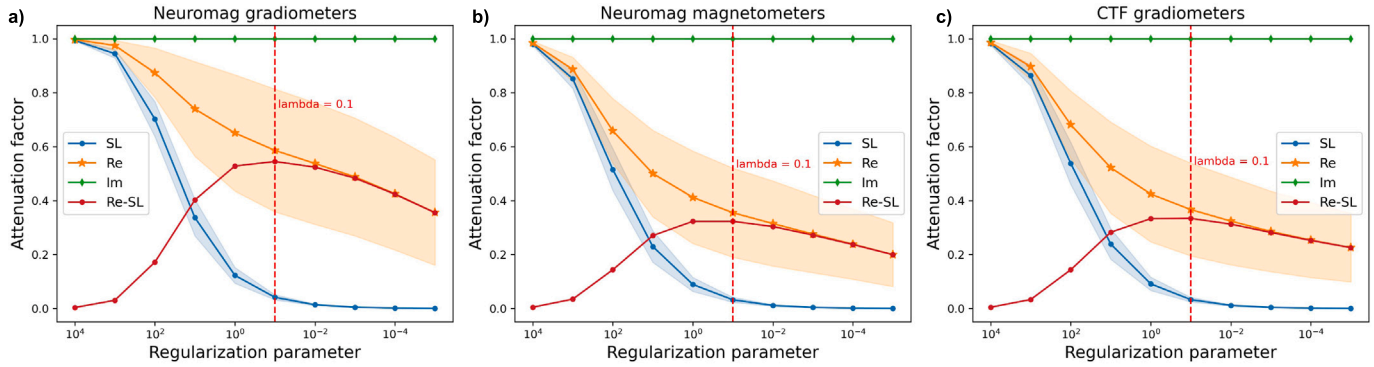

Fig. 2. SL and Re subspace power suppression and the suppression difference curve for the regularized PSIICOS as a function of the regularization parameter (a) for Neuromag 204 planar gradiometers probe, (b) for Neuromag 102 magnetometers probe and (c) for 275 radial gradiometers CTF probe.

The curves in these two figures are conceptually similar, but the latter figure corresponds to Tikhonov-regularized PSIICOS solution where the trade-off between Re and SL suppression is tuned with regularization parameter C instead of projection rank R as in Fig. 1 depicting results of Moore–Penrose pseudo-inverse based solution.

It is also possible to reformulate the constraint in (24) to specifically target the real and the imaginary parts of the source space cross-spectral coefficient c_{ij} between the time series of the ith and jth sources, see (5).

The optimal filter for the real part of the ij-th source-space cross-spectral coefficient results from imposing $\mathbf{v}_{ij}^T(\mathbf{q}_{ij}+\mathbf{q}_{ji})=1$ constraint:

$$\mathbf{v}_{ij}^{Re}=\frac{(\mathbf{\Gamma}\mathbf{\Gamma}^T+C\mathbf{I})^{-1}(\mathbf{q}_{ij}+\mathbf{q}_{ji})}{(\mathbf{q}_{ij}+\mathbf{q}_{ji})^T(\mathbf{\Gamma}\mathbf{\Gamma}^T+C\mathbf{I})^{-1}(\mathbf{q}_{ij}+\mathbf{q}_{ji})} \tag{30}$$

Correspondingly, for the imaginary part of the ij-th source-space cross-spectral coefficient with $\mathbf{v}_{ij}^T(\mathbf{q}_{ij}-\mathbf{q}_{ji})=1$ constraint we get:

$$\mathbf{v}_{ij}^{Im}=\frac{(\mathbf{\Gamma}\mathbf{\Gamma}^T+C\mathbf{I})^{-1}(\mathbf{q}_{ij}-\mathbf{q}_{ji})}{(\mathbf{q}_{ij}-\mathbf{q}_{ji})^T(\mathbf{\Gamma}\mathbf{\Gamma}^T+C\mathbf{I})^{-1}(\mathbf{q}_{ij}-\mathbf{q}_{ji})} \tag{31}$$

Note that due to the orthogonality of $(\mathbf{q}_{ij}-\mathbf{q}_{ji})$ and the column space of the spatial leakage matrix $\mathbf{\Gamma}\mathbf{\Gamma}^T$, Eq. (31) can be restated as

$$\mathbf{v}_{ij}^{Im}=\frac{(\mathbf{q}_{ij}-\mathbf{q}_{ji})}{\|(\mathbf{q}_{ij}-\mathbf{q}_{ji})\|^2} \tag{32}$$

Interestingly, filter (32) is simply a matched filter in the M^2-dimensional space and tuned to the 2-topography of the network with nodes in the ith and jth vertices of the cortical mesh. Theoretically speaking, $\mathbf{v}_{ij}^{Im}$ is a maximum-likelihood (ML) estimator of $\Im(c_{ij}^{ss})$ in the case when the observation noise is spatially white whose covariance is the identity and vanishes from the corresponding expression for the ML estimator. Filter $\mathbf{v}_{ij}^{Re}$ can also be viewed as an ML estimator of $\Re(c_{ij}^{ss})$ where the noise comes from the spatial leakage with $M^2\times M^2$ "spatial" covariance $\mathbf{\Gamma}\mathbf{\Gamma}^T$ and the additive noise term $\lambda\mathbf{I}$. Clearly, these estimators of network activity can be extended to include the information about the activity of other discrete networks, as it is done in a more traditional ML estimation of neuronal sources nicely summarized in Hauk and Stenroos (2014). For this, the set of constraints (13) and (24) needs to be augmented to include the explicit 2-topographies of the potentially interfering networks, see *Discussion* section.

The regularization parameter C in (24) plays the role of the rank parameter R in the original PSIICOS approach. By adjusting C we can softly tune the thresholding and exclude from the inversion process matrix components corresponding to low eigenvalues. Projection with rank R and the regularization based scheme can be put in correspondence by choosing for example regularization parameter C equal to the Rth singular value σ_R of $\mathbf{\Gamma}\mathbf{\Gamma}^T$ so that the corresponding eigenvalue of $C(\mathbf{\Gamma}\mathbf{\Gamma}^T+C\mathbf{I})^{-1}$ is equal to $C/(C+\sigma_R)=\sigma_R/(\sigma_R+\sigma_R)=0.5$.

The suppression factor plots sampled at the corresponding (R,C) pairs for the projected and regularized PSIICOS are shown in Fig. 3.a–c. for the Neuromag planar gradiometers, magnetometers and CTF radial gradiometers correspondingly. As expected the two approaches appear to be nearly equivalent. The suppression factor difference plots presented in panels c–f allow for selection of the optimal values controlling the regularization process in both approaches.

Note that in the above for compactness we have considered the space of sources with fixed orientations. The accommodation of the scenario with unconstrained orientations, in which the source topography is represented by the topographies of the two (in the MEG case) orthogonally oriented dipoles in the tangential plane $\mathbf{g}_i=[\mathbf{g}_i^x,\ \mathbf{g}_i^y]$, is described in the original paper (Ossadtchi et al., 2018). Instead of a single vector $\mathbf{q}_{ii}=\mathbf{g}_i\otimes\mathbf{g}_i$, we should use the triplet of vectors $\mathbf{q}_{ii}^{xx}=\mathbf{g}_i^x\otimes\mathbf{g}_i^x$, $\mathbf{q}_{ii}^{yy}=\mathbf{g}_i^y\otimes\mathbf{g}_i^y$, $\mathbf{q}_{ii}^{xy}=\mathbf{g}_i^x,\mathbf{g}_i^y+\mathbf{g}_i^y,\mathbf{g}_i^x$ per each location

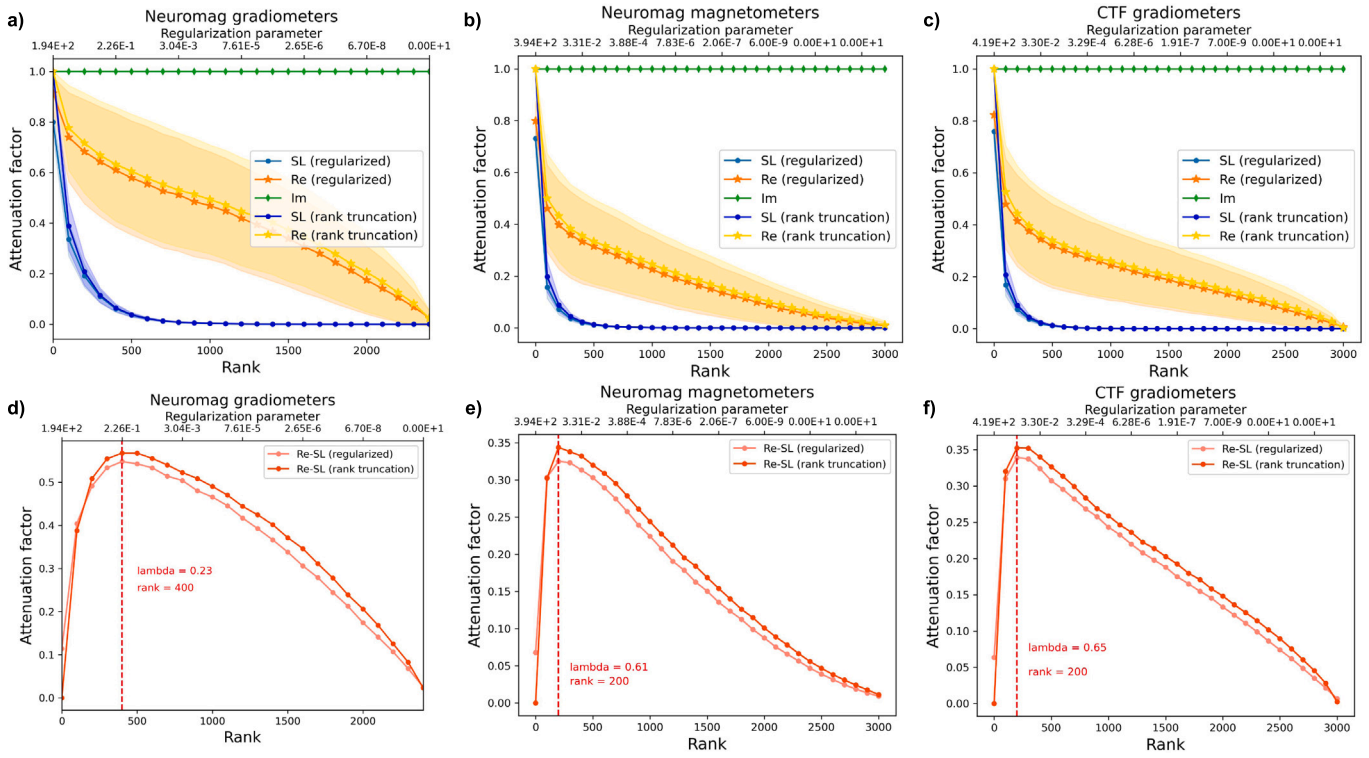

Fig. 3. SL and Re components power suppression curves (a), (b), (c), and the suppression difference curves (c), (d), (f) as functions of projection rank R and regularization parameter C. The curves are sampled at the corresponding values of the argument by choosing $C = \sigma_R$ for 204 Neuromag planar gradiometers probe (a,d), 102 Neuromag magnetometers probe (b, e) and 275 radial gradiometers CTF probe (c, f).

when creating matrix $\mathbf{\Gamma}$, see (10). These vectors span the SL subspace of the ith source and enter into matrix $\mathbf{\Gamma}$. The projection away from the space spanned by these three vectors cancels the contribution to SL of an arbitrarily oriented source located in the ith vertex. .

3. Lower rank approximation

The vast majority of methods for the source-space functional coupling assessment is based on precomputing the source time series using an inverse solver of choice or using direct source space estimation followed by computing the statistics of interest. For example, the DICS (Großet al., 2001) technique is based on the analysis of the estimate of the source space cross-spectral coefficient c_{ij} obtained as

$$c_{ij}(f,t) = \mathbf{w}_i^T \mathbf{C}^{XX}(f,t)\mathbf{w}_j = (\mathbf{w}_j \otimes \mathbf{w}_i)^T vec\left(\mathbf{C}^{XX}(f,t)\right) \tag{33}$$

where $\mathbf{w}_i$ and $\mathbf{w}_j$ are the spatial filters tuned for the ith and jth source respectively. Note that although this may not be evident but the DICS expression compactly represents the two step procedure where $c_{ij}(f,t)$ is computed simply as the expectation of the time–frequency transformed estimates of time series of the ith and jth sources obtained with spatial filters $\mathbf{w}_i$ and $\mathbf{w}_j$ correspondingly. To see this one can write $\mathbf{w}_i^T \mathbf{C}^{XX}(f,t)\mathbf{w}_j = \mathbf{w}_i^T E\{\mathbf{x}(f,t)\mathbf{x}^H(f,t)\}\mathbf{w}_j = E\{\mathbf{w}_i^T \mathbf{x}(f,t)\mathbf{x}^H(f,t)\mathbf{w}_j\} = E\{S_i(f,t)S_j^*(f,t)\}$ and therefore the quality of such an assessment is fully determined by the properties of the spatial filters $\mathbf{w}_i$ and $\mathbf{w}_j$ used to estimate the time series of the ith and the jth source.

The operation described by (33) can be restated as

$$\begin{aligned} c_{ij}(f,t) &= \mathbf{w}_i^T \mathbf{C}^{XX}(f,t)\mathbf{w}_j = (\mathbf{w}_j \otimes \mathbf{w}_i)^T vec\left(\mathbf{C}^{XX}(f,t)\right) \\ &= \mathbf{w}_{ij}^{1T} vec\left(\mathbf{C}^{XX}(f,t)\right) \end{aligned} \tag{34}$$

Vector $\mathbf{w}_{ij}^1$ represents a filter operating in the M^2 dimensional space and acting on the vectorized cross-spectrum $vec\left(\mathbf{C}^{XX}(f,t)\right)$. In the traditional connectivity estimation setting (33) this filter has a special constraint that forces it to be expressed as a Kronecker product of two M-dimensional vectors, e.g. $\mathbf{w}_{ij}^1 = vec(\mathbf{w}_i \mathbf{w}_j^T) = \mathbf{w}_j \otimes \mathbf{w}_i$. In what follows this particular structure will be denoted as the rank-1 form.

As demonstrated in the previous sections the PSIICOS approach relaxes this constraint on the spatial filter structure and seeks for a $M^2 \times 1$ $\mathbf{w}_{ij}$ to optimize the trade-off between the extent of the mutual leakage suppression and the amount of the retained power modulated by the real component of the source-space cross-spectrum. The latter is achieved either by adjusting the projection rank R or the regularization parameter C whose conceptual equivalence was demonstrated in Fig. 3. Operation in the M^2 dimensional space endows PSIICOS with extra power in suppressing the mutual spatial leakage component as compared to the traditional processing described by Eq. (33). It allows PSIICOS to efficiently attenuate the mutual spatial leakage (9) in a principled way and retain information about the sensor-space cross-spectral components modulated by the real part of the source-space cross-spectrum.

How much fidelity in suppressing the SL will be lost if we approximate the PSIICOS filter using rank-1 representation? To answer this question we first need to come up with an approximation quality criterion Q. One possible approach is to gauge the approximation quality using the norm of the difference between the original $\mathbf{w}_{ij}$ and the rank-1 approximated PSIICOS filter $\mathbf{w}_{ij}^1$. We dub this approach as "naive" for the reasons that will become clear later, $Q_{naive} = \|\mathbf{w}_{ij} - \mathbf{w}_{ij}^1\|$. Optimizing Q_{naive} leads to the following algorithm for building a rank-1 approximation of $\mathbf{w}_{ij} \approx \mathbf{w}_{ij}^1 = \tilde{\mathbf{w}}_j \otimes \tilde{\mathbf{w}}_i = vec\left(\tilde{\mathbf{w}}_i \tilde{\mathbf{w}}_j^T\right)$:

- Reshape PSIICOS $\mathbf{w}_{ij}$ into a $M \times M$ matrix $\mathbf{W}_{ij}$
- In order to find such $\tilde{\mathbf{w}}_i$ and $\tilde{\mathbf{w}}_j$ that $\|\mathbf{w}_{ij} - \tilde{\mathbf{w}}_i \tilde{\mathbf{w}}_j^T\|_F$ is minimum use the defining property of the SVD and represent $\mathbf{W}_{ij}$ as $\mathbf{W}_{ij} = \mathbf{USV}^T$, with $\mathbf{U} = [\mathbf{u}_1 \mathbf{u}_2, \ldots, \mathbf{u}_M]$, $\mathbf{V} = [\mathbf{v}_1 \mathbf{v}_2, \ldots, \mathbf{v}_M]$, $\mathbf{S} = \mathbf{diag}([s_1, s_2, \ldots, s_M])$
- Compute rank-1 approximation of $\mathbf{w}_{ij}$ as $\mathbf{w}_{ij}^1 = s_1 \mathbf{v}_1 \otimes \mathbf{u}_1$ as the vectorized outer product of the first pair of singular vectors

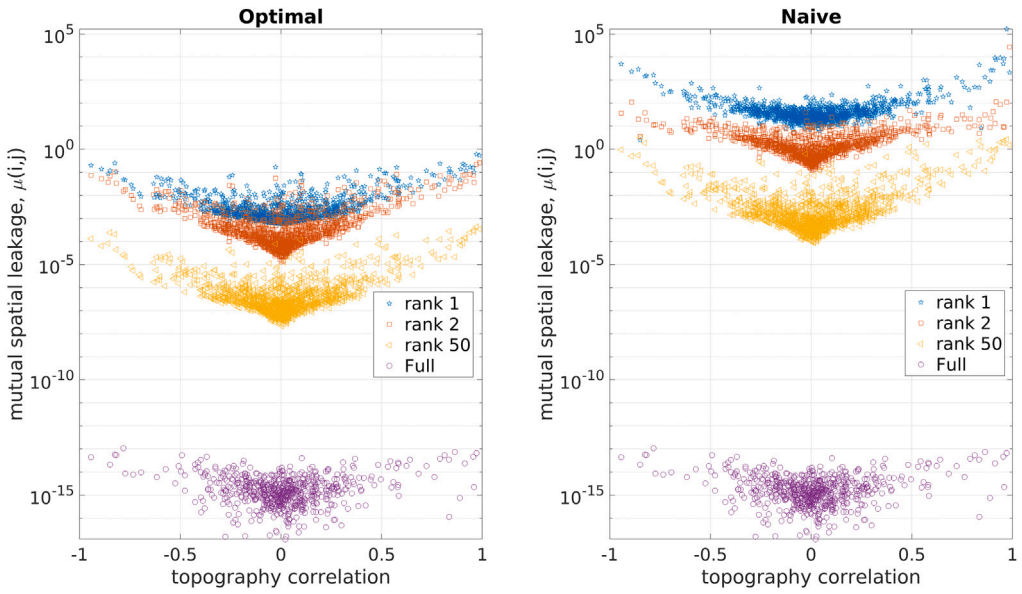

Fig. 4. Optimal vs. naive lower rank approximation of PSIICOS filters. The ordinate of the dots in this plot corresponds to the mutual spatial leakage $\mu^r(i,j)$ computed as $\tilde{\mathbf{w}}_{ij}^r T(\mathbf{\Gamma\Gamma^T})\tilde{\mathbf{w}}_{ij}^r$ for different approximation ranks $r = 1, 2, 50$ and for the full rank. We have also normalized each approximation to ensure the unity gain constraint in the "direction" of the 2-topography $\mathbf{g}_j \otimes \mathbf{g}_i + \mathbf{g}_i \otimes \mathbf{g}_j$ of the real part of the source space cross-spectral c_{ij} coefficient. Each dot corresponds to a randomly chosen pair (i,j) of cortical sources. Dot's position along the horizontal axis is determined by the correlation coefficient of the ith and the jth source topographies $\rho = \mathbf{g}_i^T \mathbf{g}_j / \|\mathbf{g}_i\| \|\mathbf{g}_j\|$. As we can see the optimal scheme (on the left) allows for a stronger attenuation of the mutual spatial leakage as compared to the naive scheme (on the right).

corresponding to the largest singular value s_1 and assign $\tilde{\mathbf{w}}_i = \sqrt{s_1}\mathbf{u}_1$ and $\tilde{\mathbf{w}}_j = \sqrt{s_1}\mathbf{v}_1$

- Higher rank approximations can also be computed as $\mathbf{w}_{ij}^R = \sum_{r=1}^R s_r \mathbf{v}_r \otimes \mathbf{u}_r$

Per defining property of SVD the above approach minimizes the residual difference $\|\mathbf{w}_{ij} - \mathbf{w}_i \tilde{\mathbf{w}}_j^T\|_F^2 = \|\mathbf{w}_{ij} - \mathbf{w}_{ij}^1\|_F^2 = (\mathbf{w}_{ij} - \mathbf{w}_{ij}^1)^T(\mathbf{w}_{ij} - \mathbf{w}_{ij}^1) = Q_{naive}$ which does not control the extent to which the mutual spatial leakage $\mu(i,j)$ is suppressed. The above approximation scheme can be improved to take this into account in order to obtain a better approximation. To control $\mu(i,j)$ and achieve the best low rank approximation of a filter in the sense of retaining maximum of the SL attenuation we will reformulate our approximation quality criterion as

$$Q = (\mathbf{w}_{ij} - \tilde{\mathbf{w}}_i \otimes \tilde{\mathbf{w}}_j)^T (\mathbf{\Gamma\Gamma^T})(\mathbf{w}_{ij} - \tilde{\mathbf{w}}_i \otimes \tilde{\mathbf{w}}_j) =$$
$$= \left[(\mathbf{w}_{ij} - \tilde{\mathbf{w}}_i \otimes \tilde{\mathbf{w}}_j)\left(\mathbf{\Gamma\Gamma^T}\right)^{1/2}\right]^T \left[(\mathbf{w}_{ij} - \tilde{\mathbf{w}}_i \otimes \tilde{\mathbf{w}}_j)\left(\mathbf{\Gamma\Gamma^T}\right)^{1/2}\right]. \quad (35)$$

Q in (35) can be optimized in much the same way as Q_{naive} except that prior to reshaping and performing the SVD the original filter $\mathbf{w}_{ij}$ needs to be multiplied by the scaling matrix $\mathbf{H} = (\mathbf{\Gamma\Gamma^T})^{1/2}$. After the SVD, the obtained lower rank approximation needs to be reshaped and multiplied back by the inverse of $\mathbf{H}$.

The left and the right panels of Fig. 4 compare the two lower rank approximation methods by visualizing the extent to which the spatial leakage (SL) subspace variance projects onto the specific filter designed to recover source space cross-spectral coefficient c_{ij} for a randomly chosen pair of cortical vertices (i,j). The ordinate of the dots in this plot corresponds to the amount of mutual leakage $\mu^r(i,j) = \mathbf{w}_{ij}^{rT}(\mathbf{\Gamma\Gamma^T})\mathbf{w}_{ij}^r$ for $r = 1, 2, 50$ and for the full rank and measures the amount of average residual spatial leakage power after applying the PSIICOS filter. The abscissa of each dot reflects the correlation coefficient of the topographies of sources located in the ith and jth vertex. We have also normalized each approximation to ensure the unity gain constraint in the "direction" of the 2-topography $\mathbf{g}_j \otimes \mathbf{g}_i + \mathbf{g}_i \otimes \mathbf{g}_j$ modulated by the real part of the source space cross-spectrum c_{ij} coefficient. As we can see the second scheme (on the left) achieves smaller $\mu^r(i,j)$ for all approximation ranks r as compared to the naive approach (on the right).

In Ossadtchi et al. (2018) the authors suggested conducting a reduced version of the MUSIC scan to identify active networks. Since the MUSIC family of techniques is highly sensitive to the forward model accuracy when evaluating the quality of the approximation, we must consider the forward model similarity metric alongside the mutual spatial leakage suppression criterion. PSIICOS filters $\mathbf{v}_{ij}$ are basically matched filters tuned to the SL-debiased 2-topography and we will measure the cosine of the angle between the approximated and the original filter as $\theta_{ij} = \mathbf{v}_{ij}^T \mathbf{w}_{ij}^r / \|\mathbf{w}_{ij}^r\| \|\mathbf{v}_{ij}^r\|$. Fig. 5.a shows the distribution of θ_{ij} for a set of randomly selected pairs (i,j) of cortical locations. As in Fig. 4.a the horizontal coordinate corresponds to the ith and jth topography correlation coefficient $\rho_{ij} = \mathbf{g}_i^T \mathbf{g}_j / \|\mathbf{g}_i\| \|\mathbf{g}_j\|$. We can see that the increase of the approximation rank reduces the fraction of examples with low cosine similarity. Typically, locating cortical sources using the MUSIC technique requires subspace correlation values above 0.95, which means that the obtained rank-1 approximation is likely not sufficient to reliably identify networks whose activity is manifested in the observed sensor-space cross-spectrum.

Fig. 5.b provides an easy-to-understand summary of our results for this section. Each dot in the graph corresponds to a randomly chosen pair of cortical locations (i,j). The mutual spatial leakage $\mu^r(i,j)$ and cosine similarity criteria are used as coordinates for the dots. As the rank of the approximation increases, the distribution of dots becomes more horizontal around $cos(\mathbf{w}_{ij}, \mathbf{w}_{ij}^R) = 1$ and shifts towards the left indicating average mutual spatial leakage reduction.

4. Discussion

In this theoretical paper we presented a proof of optimality of PSIICOS, the framework that has been empirically introduced by us earlier (Ossadtchi et al., 2018). PSIICOS was designed to provide better sensitivity to the networks coupled at zero- or close to zero phase lag as compared to more traditional approaches exploiting the imaginary part of the cross-spectrum. In Ossadtchi et al. (2018) we conducted a series of experiments with simulated data to compare PSIICOS against more commonly used techniques such as DICS, iDICS and geometric correction scheme (GCS). The simulations confirmed nearly uniform sensitivity of PSIICOS to the phase between the time series of the functionally coupled nodes. We have also applied PSIICOS to real MEG

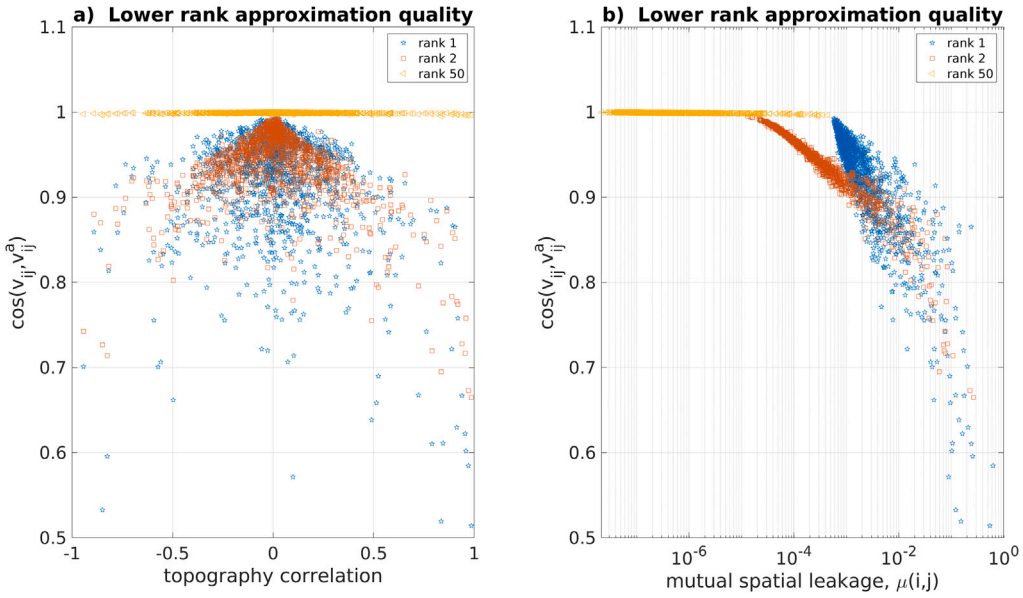

Fig. 5. Lower rank approximation quality assessment. (a) The distribution of θ_{ij} for a set of randomly selected cortical location pairs (i, j). The horizontal coordinate corresponds to the ith and jth topography correlation coefficient ρ. The increase of the approximation rank reduces the fraction of examples with low cosine similarity. (b) Cosine similarity vs SL attenuation for a set of randomly chosen cortical location pairs (i, j). The increase of the approximation rank orients the distribution of points more horizontally and shifts it to the left.

data recorded during mental rotation experiment and obtained several physiologically plausible networks. Interestingly, we observed better stability of the networks characterized by low phase delay that are most strongly manifested in the SL-debiased real part of the cross-spectrum. Another notable benefit of PSIICOS is that its computational requirements are modest. Creating the projection matrix $\mathbf{P}$ for a forward model with 1500 cortical vertices takes around 7 s on a regular PC and needs to be done only once for a given forward model. The vectorized scan over 1500 × 1500 pairs takes on the order of 0.5 s on the same machine. Taken together, the empirical advantages of PSIICOS are apparent.

Within the scope of this paper, we have demonstrated that the PSIICOS projection is optimal in the sense of minimizing the overlap between beam response vectors corresponding to the cortical locations evaluated for functional connectivity. To this end we have first derived the mutual spatial leakage criteria that uses modified resolution matrix (Samuelsson et al., 2021). This criteria is similar to that used by Nolte et al. (2009), Marzetti et al. (2008) to reflect the properties of the hypothesized underlying ground truth distribution of neuronal sources.

The direct assessment of the spatial structure of mutual spatial leakage became possible, as PSIICOS operates in the M^2 dimensional product space of sensor signals. This assessment includes identifying a set of complementary subspaces capturing the largest mutual spatial leakage variance for a given subspace rank. This approach facilitates tuning the mutual spatial leakage subspace rank to balance between suppressing mutual spatial leakage and retaining information about the real part of the source-space cross-spectrum.

In the extreme case PSIICOS projection leads to a complete depletion of mutual spatial leakage power, resulting in the established approaches that rely solely on the imaginary part of the sensor-space cross-spectrum (Nolte et al., 2004). However, these techniques fail to detect functional networks with nodes coupled at or near zero phase lags since this information is stored in the real part of the cross-spectrum.

It is important to realize that a direct application of an inverse solver to PSIICOS projected sensor-space cross-spectral matrix would result in a non positive definite matrix that cannot be interpreted as a source space cross-spectral matrix. Instead we profess an alternative view to the estimation of source space cross-spectral coefficients reflecting the FC. Assuming sufficient suppression of the SL component, the vector of projected sensor-space cross-spectrum is basically a linear combination of projected 2-topographies corresponding to the pairs of coupled sources. The coefficients of this linear combination are the real and imaginary parts of the source-space pairwise cross-spectrum. The FC estimation problem lies then in assessing the coefficients of this linear combination.

In other words, instead of the concept of a neuronal source approximated by a single equivalent current dipole (ECD) in the conventional inverse problem framework, the PSIICOS paradigm uses the notion of *dyadic network* whose nodes are two ECDs located at two disjoint locations of the cortex. Instead of conventional source topography $\mathbf{g}_i$ corresponding to an individual ECD, the PSIICOS operates with dyadic network (a pair of ECDs) as "sources" whose manifestation in the sensor-space is described by 2-topographies computed as $\mathbf{g}_j \otimes \mathbf{g}_i$ using the Kronecker product of conventional ECD topographies of the ith and the jth source forming the elementary dyadic network. Finally, instead of source activation time series, the PSIICOS framework employs cross-spectral coefficient time series $c_{ij}(t, f)$, that characterize the functional coupling within the elementary network formed by the ith and the jth cortical source, see Eq. (6).

This view highlights the similarity between the FC estimation problem based on the PSIICOS projected cross-spectrum and the classical source estimation problem defined by the generative Eq. (3). PSIICOS framework allows us to view the FC estimation task also as a regression problem but centered not on the equivalent current dipoles with topographies $\mathbf{g}_i$ and activations $S_i^k(f, t)$ but rather on the elementary *dyadic networks* whose activity is described by the cross-spectral coefficients $c_{ij}^{ss}(f, t)$ and gets mapped to the sensor space with 2-topographies, see Eq. (10).

In this light the solutions (30) and (32) are basically maximum likelihood (ML) estimators of the real and imaginary parts of the $c_{ij}(f, t)$, see equation (16) in Hauk and Stenroos (2014). The noise covariance matrix in (30) is formed by the mutual spatial leakage matrix $\mathbf{\Gamma}\mathbf{\Gamma}^T$ and the added white noise term $C\mathbf{I}$ used for regularization. As an ML estimator, the algorithm basically performs matched filtering in the space whitened by the inverse square root of $\mathbf{C}_N = \mathbf{\Gamma}\mathbf{\Gamma}^T + C\mathbf{I}$ noise covariance matrix. Solution (32) also represents a matched filter

tuned to the 2-topography $\mathbf{q}_{ij} - \mathbf{q}_{ji}$ whose contribution to the sensor-space cross-spectrum is modulated by the imaginary part of c_{ij}. In this case the noise covariance $\mathbf{C}_N$ is the identity matrix, i.e. $\mathbf{C}_N = \mathbf{I}$, which reflects the fact that the spatial leakage does not affect the imaginary part of the cross-spectrum. In fact, the estimates of $\Im(c_{ij})$ delivered by PSIICOS match those obtained with a more conventional imaginary DICS approach (Nolte et al., 2004; Ossadtchi et al., 2018).

It is important to mention the possible extensions of PSIICOS approach and its incorporation to the standard frameworks. One of the most descriptive examples is integration of PSIICOS with an arbitrary linear inverse operator presented by Hindriks (2020). PSIICOS was additionally adjusted to incorporate SL suppression using either the source-space cross-spectrum derived from the reconstructed source time series or the source-space cross-spectrum obtained from inverse modeling utilizing the uncorrected sensor-space cross-spectrum. All three approaches of combining PSIICOS with inverse operators successfully identified source interactions independent of the lags.

At the same time, the utilization of sensor-based estimates with correction in the source space was found to be slightly more advantageous in suppressing the SL, but the differences between the three correction scenarios were relatively small as all of them provided a significant suppression of the SL. Such small differences between the three possible variants of linear approaches to SL suppression using PSIICOS may indirectly suggest that PSIICOS is the optimal linear method for effectively minimizing mutual spatial leakage. Interestingly, Hindriks (2020) also observed that the use of the sensor-space cross-spectral estimates with correction in the source space eliminates the first-order spurious interactions and allows for reconstruction of functional networks with more than two sources.

The applications of the PSIICOS approach can extend to the space of cortical parcels. The solution aimed at the simultaneous optimization of the inverse solver to extract phase evolution time series of sources located in a pair of cortical patches has been previously described in Korhonen et al. (2014). The authors derive sparse weights to collapse a cortical patch comprising multiple ECDs into a smaller set of ECDs such that the pairwise phase synchrony profiles computed based on the reconstructed time series of such collapsed patches match the simulated ground truth values. Another related approach is based on using patches that are not solely determined by anatomical boundaries but modified based on the optimization of the cross-talk function, which enables the reduction of leakage between the parcels (Farahibozorg et al., 2018). In the future the enhancement of cross-talk function optimization can be achieved through the utilization of a PSIICOS projector designed to effectively suppress both inter-patch and within-patch leakage.

Overall, the PSIICOS approach proposes a shift from the traditional two-step functional connectivity estimation procedure to operating in the M^2-dimensional space of sensor-space cross-spectrum. This view allows us to highlight the fact that the classical two-step approach of connectivity estimation is simply a matched filter that focuses on the topographies of the corresponding networks without considering the interference structure and therefore can be improved. PSIICOS implements only the most straightforward improvement and relaxes the requirement on the rank-1 structure of the filter. The future endeavors also include formulation of fully fledged Bayesian estimators of connectivity as a dynamic variable that take into account *apriori* information derived from the structural connectome data. These novel methods will exploit the rich intuition accumulated in the community with respect to the traditional source estimation tasks (Hauk and Stenroos, 2014).

Funding

The study was implemented in the framework of the Basic Research Program at the National Research University Higher School of Economics (HSE University), Russia in 2023.

CRediT authorship contribution statement

Dmitrii Altukhov: Conceptualization, Mathematical derivations, Writing. **Daria Kleeva:** Simulations, Writing. **Alexei Ossadtchi:** Conceptualization, Mathematical derivations, Simulations, Writing, General coordination.

Declaration of competing interest

The authors declare that they have no conflicts of interest regarding the publication of this article.

Data availability

Data will be made available on request.

References

Aydore, S., Pantazis, D., Leahy, R.M., 2013. A note on the phase locking value and its properties. Neuroimage 74, 231–244.

Bastos, A.M., Schoffelen, J.-M., 2016. A tutorial review of functional connectivity analysis methods and their interpretational pitfalls. Front. Syst. Neurosci. 9, 175.

Bowyer, S.M., 2016. Coherence a measure of the brain networks: Past and present. Neuropsychiatric Electrophysiol. 2, 1–12.

Ewald, A., Marzetti, L., Zappasodi, F., Meinecke, F.C., Nolte, G., 2012. Estimating true brain connectivity from EEG/MEG data invariant to linear and static transformations in sensor space. Neuroimage 60 (1), 476–488.

Farahibozorg, S.-R., Henson, R.N., Hauk, O., 2018. Adaptive cortical parcellations for source reconstructed EEG/MEG connectomes. NeuroImage 169, 23–45.

Fries, P., 2015. Rhythms for cognition: Communication through coherence. Neuron 88 (1), 220–235.

Gail, A., Brinksmeyer, H.J., Eckhorn, R., 2004. Perception-related modulations of local field potential power and coherence in primary visual cortex of awake monkey during binocular rivalry. Cerebral Cortex 14 (3), 300–313.

Greicius, M., 2008. Resting-state functional connectivity in neuropsychiatric disorders. Curr. Opin. Neurol. 21 (4), 424–430.

Groß, J., Kujala, J., Hämäläinen, M., Timmermann, L., Schnitzler, A., Salmelin, R., 2001. Dynamic imaging of coherent sources: Studying neural interactions in the human brain. Proc. Natl. Acad. Sci. 98 (2), 694–699.

Hauk, O., Stenroos, M., 2014. A framework for the design of flexible cross-talk functions for spatial filtering of EEG/MEG data: DeFleCT. Hum. Brain Map. 35 (4), 1642–1653.

Hauk, O., Stenroos, M., Treder, M.S., 2022. Towards an objective evaluation of EEG/MEG source estimation methods–The linear approach. Neuroimage 255, 119177.

Hincapie, A.-S., Kujala, J., Mattout, J., Pascarella, A., Daligault, S., Delpuech, C., Mery, D., Cosmelli, D., Jerbi, K., 2017. The impact of MEG source reconstruction method on source-space connectivity estimation: A comparison between minimum-norm solution and beamforming. Neuroimage 156, 29–42.

Hindriks, R., 2020. Lag-invariant detection of interactions in spatially-extended systems using linear inverse modeling. PLoS One 15 (12), e0242715.

Hindriks, R., Tewarie, P.K., 2023. Dissociation between phase and power correlation networks in the human brain is driven by co-occurrent bursts. Commun. Biol. 6 (1), 286.

Hutchison, R.M., Womelsdorf, T., Allen, E.A., Bandettini, P.A., Calhoun, V.D., Corbetta, M., Della Penna, S., Duyn, J.H., Glover, G.H., Gonzalez-Castillo, J., et al., 2013. Dynamic functional connectivity: Promise, issues, and interpretations. Neuroimage 80, 360–378.

Korhonen, O., Palva, S., Palva, J.M., 2014. Sparse weightings for collapsing inverse solutions to cortical parcellations optimize M/EEG source reconstruction accuracy. J. Neurosci. Methods 226, 147–160.

Marzetti, L., Del Gratta, C., Nolte, G., 2008. Understanding brain connectivity from EEG data by identifying systems composed of interacting sources. Neuroimage 42 (1), 87–98.

Nolte, G., Bai, O., Wheaton, L., Mari, Z., Vorbach, S., Hallett, M., 2004. Identifying true brain interaction from EEG data using the imaginary part of coherency. Clin. Neurophysiol. 115 (10), 2292–2307.

Nolte, G., Marzetti, L., Sosa, P.V., 2009. Minimum overlap component analysis (MOCA) of EEG/MEG data for more than two sources. J. Neurosci. Methods 183 (1), 72–76.

Nolte, G., Ziehe, A., Nikulin, V.V., Schlögl, A., Krämer, N., Brismar, T., Müller, K.-R., 2008. Robustly estimating the flow direction of information in complex physical systems. Phys. Rev. Lett. 100 (23), 234101.

Ossadtchi, A., Altukhov, D., Jerbi, K., 2018. Phase shift invariant imaging of coherent sources (PSIICOS) from MEG data. NeuroImage 183, 950–971.

Pascual-Marqui, R.D., Lehmann, D., Koukkou, M., Kochi, K., Anderer, P., Saletu, B., Tanaka, H., Hirata, K., John, E.R., Prichep, L., et al., 2011. Assessing interactions in the brain with exact low-resolution electromagnetic tomography. Phil. Trans. R. Soc. A 369 (1952), 3768–3784.

Samuelsson, J.G., Peled, N., Mamashli, F., Ahveninen, J., Hämäläinen, M.S., 2021. Spatial fidelity of MEG/EEG source estimates: A general evaluation approach. Neuroimage 224, 117430.

Sekihara, K., Nagarajan, S.S., 2008. Adaptive Spatial Filters for Electromagnetic Brain Imaging. Springer Science & Business Media.

Siegel, M., Donner, T.H., Engel, A.K., 2012. Spectral fingerprints of large-scale neuronal interactions. Nat. Rev. Neurosci. 13 (2), 121–134.

Stam, C.J., Nolte, G., Daffertshofer, A., 2007. Phase lag index: Assessment of functional connectivity from multi channel EEG and MEG with diminished bias from common sources. Hum. Brain Map. 28 (11), 1178–1193.

Varela, F., Lachaux, J.-P., Rodriguez, E., Martinerie, J., 2001. The brainweb: Phase synchronization and large-scale integration. Nature Rev. Neurosci. 2 (4), 229–239.

Westner, B.U., Dalal, S.S., Gramfort, A., Litvak, V., Mosher, J.C., Oostenveld, R., Schoffelen, J.-M., 2022. A unified view on beamformers for M/EEG source reconstruction. Neuroimage 246, 118789.

Zeitler, M., Fries, P., Gielen, S., 2006. Assessing neuronal coherence with single-unit, multi-unit, and local field potentials. Neural Comput. 18 (9), 2256–2281.